Quantum anomalous Hall effect in $MnBi_2Te_4$ van der Waals heterostructures

Ruiling Gao,[1] Guanhua Qin,[1] Shifei Qi,[2,3,*] Zhenhua Qiao,[3,†] and Wei Ren[1,‡]

[1]*Physics Department, State Key Laboratory of Advanced Special Steel, Shanghai Key Laboratory of High Temperature Superconductors, MGI and ICQMS, Shanghai University, Shanghai 200444, China*

[2]*College of Physics and Hebei Advanced Thin Film Laboratory, Hebei Normal University, Shijiazhuang 050024, Hebei, China*

[3]*ICQD, Hefei National Laboratory for Physical Sciences at Microscale, CAS Key Laboratory of Strongly-Coupled Quantum Matter Physics, and Department of Physics, University of Science and Technology of China, Hefei, Anhui 230026, China*

(Received 28 May 2021; revised 9 September 2021; accepted 5 October 2021; published 5 November 2021)

Quantum anomalous Hall effect (QAHE) has been experimentally realized in the intrinsic antiferromagnetic topological insulator $MnBi_2Te_4$. However, at ambient condition the magnetization of the $MnBi_2Te_4$ sample decreases significantly after it is exposed in air for a couple of days, which hinders its potential application. Here, we theoretically propose to cover 2D van der Waals materials such as hexagonal boron nitride (h-BN) monolayer onto the surface of $MnBi_2Te_4$. This not only protects the stability of $MnBi_2Te_4$, but also leads to interlayer ferromagnetic coupling and further realizes the QAHE at higher temperature. We find that interlayer ferromagnetic transition occurs generally when monolayer h-BN, MoS_2, or WSe_2 is covered onto two or three septuple-layer $MnBi_2Te_4$ with interlayer antiferromagnetic coupling. Band-structure and topological properties calculations show that h-BN/$MnBi_2Te_4$ heterostructure exhibits a topologically nontrivial band gap around 64–75 meV, hosting QAHE with a Chern number of $C = 1$. Our proposed materials system should be considered as an ideal platform to explore high-temperature QAHE due to their relatively simple and stable structures.

DOI: 10.1103/PhysRevMaterials.5.114201

I. INTRODUCTION

Quantum anomalous Hall effect (QAHE) induced by the intrinsic long-range ferromagnetism and spin-orbit coupling, depends essentially on the topologically nontrivial electronic structure but without necessity of an external magnetic field [1–5]. Thanks to its robustness against backscattering, the dissipationless chiral edge states are attractive for applications in next-generation low-power consumption nanoelectronic devices [2,6]. Haldane first proposed a honeycomb lattice toy model for the QAHE without Landau levels caused by strong magnetic field [1]. Thereafter, there have been numerous efforts to search new systems for realizing the QAHE [7–18]. Among these proposals, using magnetically doped Z_2 topological insulator (TI) which has inherently strong spin-orbit coupling is one of the most common routes [8–10,19–21]. This approach has indeed been verified experimentally, where a quantized conductance plateau could be observed in magnetically doped TI (Cr-doped $Bi_xSb_{2-x}Te_3$) film for the first time in 2013 [22]. However, the observation temperature of QAHE in experiment is as extremely low as 300 mK [23], which greatly limits the application of QAHE and therefore there is an urgent need to increase it.

In addition to introducing magnetic dopants into TIs, it is also possible to employ magnetic proximity to construct TI/magnetic insulator heterojunctions [14,24–28] with higher Curie temperature [29]. However, due to the complex interaction at the heterojunction interface, the quantized conductance was not easy to be observed experimentally [30–32]. In order to better control the heterostructures, van der Waals (vdW) layered materials have attracted increasing attention. Recently, both experiment and theory reports have successfully confirmed $MnBi_2Te_4$ (MBT) to be an intrinsic magnetic topological insulator, as a vdW layered compound with hexagonal lattice [33,34]. It consists of seven atomic layers of Te-Bi-Te-Mn-Te-Bi-Te to form a basic septuple-layer (SL) unit, as shown in Fig. 1. Based on its intralayer ferromagnetic (FM) and interlayer antiferromagnetic (AFM) couplings, MBT exhibits very rich topological states. For example, when the layer thickness number is an odd multiple of SLs, the system is the quantum anomalous Hall phase; otherwise, it is the axion insulator phase and exhibits topological magnetoelectric effect characteristics [33]. Therefore, there has been intensive investigation on its physical properties, especially about the QAHE [35–37]. A zero-field quantized conductance plateau was successfully observed at 4.5 K, and an additional magnetic field applied to the MBT could transform it from an antiferromagnetic state to a ferromagnetic state [38]. Clearly, in order to realize QAHE for the MBT system under zero magnetic field, the inherent interlayer antiferromagnetic coupling is an undesired obstacle. In addition, MBT films are prone to degrade at ambient condition; the magnetization M_s of MBT sample decreases significantly after it is exposed in air for a couple of days [34,39–41]. Therefore, finding an effective way to protect the material is also crucial for the experimental investigations. The relatively stable 2D vdW materials, such as h-BN [42,43], MoS_2 [44], and WSe_2 [45], have been

*qisf@hebtu.edu.cn
†qiao@ustc.edu.cn
‡renwei@shu.edu.cn

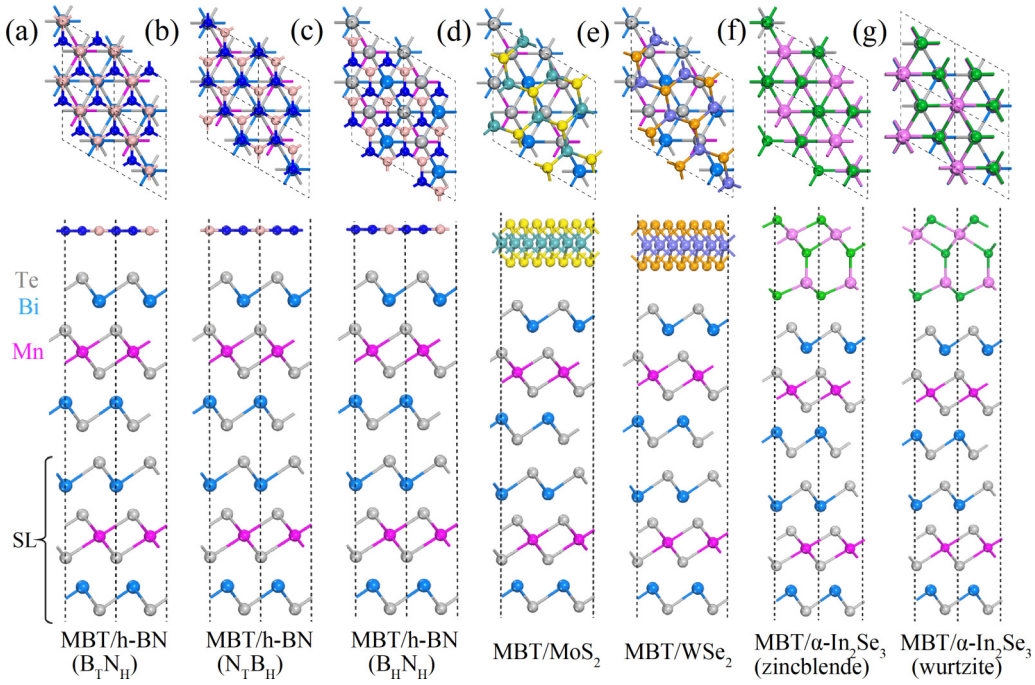

FIG. 1. Top and side views of vdW heterostructures consisting of different 2D materials on top of 2SL $MnBi_2Te_4$. (a) h-BN (B_TN_H), (b) h-BN (N_TB_H), (c) h-BN (B_HN_H), (d) MoS_2, (e) WSe_2, (f) zincblende, and (g) wurtzite α-In_2Se_3 structures.

successfully exfoliated experimentally thanks to their weak vdW interlayers interaction. In addition, experiments [46] and theories [47] have demonstrated that h-BN/phosphorene/h-BN heterostructures devices exist stably in the air by encapsulating unstable phosphorene within h-BN.

In this paper, by performing the first-principles density-functional theory (DFT) calculation, we show that MBT/2D vdW heterostructures not only effectively protect MBT, but also assist interlayer ferromagnetic transition for achieving higher-temperature QAHE. This is generally possible when a monolayer vdW material, such as h-BN, MoS_2, and WSe_2, is used to cover onto MBT having interlayer antiferromagnetic coupling. Moreover, our DFT calculations show that band structures of 2SL or 3SL MBT/h-BN heterostructure manifest topologically nontrivial band gaps about 64–75 meV depending on different ways of stacking and thickness of MBT, while hosting QAHE with a Chern number of $C = 1$. Therefore, based on their simple and stable heterostructures, our proposed systems should be excellent candidates to realize high-temperature QAHE.

II. METHODS

Our first-principles calculations were performed using the projected augmented-wave method as implemented in the Vienna *Ab initio* Simulation Package (VASP) [48,49]. The generalized gradient approximation (GGA) of Perdew-Burke-Ernzerhof type was used to treat the exchange-correlation interaction [50]. After building seven different heterostructures with h-BN, MoS_2, WSe_2, α-In_2Se_3, and MBT, we have carried out a systematic investigation on them. We considered three different structures that are composed of the following unit cells: $\sqrt{3}\times\sqrt{3}$ h-BN and 1×1 MBT, for different stacking; $\sqrt{7}\times\sqrt{7}$ MoS_2 and 2×2 MBT; $\sqrt{7}\times\sqrt{7}$ WSe_2 and 2×2 MBT; two structures of 1×1 α-In_2Se_3 and 1×1 MBT, for two different phases of α-In_2Se_3. A vacuum buffer space of 15 Å was used to prevent coupling between adjacent slabs. The kinetic energy cutoff was set to 450 eV. The optimal lattice constants $a = b = 4.334$ Å of 2SL MBT are obtained through energy calculation, consistent with the available experimental [51] and theoretical values [52–54]. All heterojunctions models are constructed by fixing the lattice parameter of MBT and stretching or compressing other 2D materials. All the internal atomic coordinates in the heterojunction systems have been fully optimized. During structural relaxation, all atoms were allowed to relax until the Hellmann-Feynman force on each atom was less than 0.01 eV/Å. The Brillouin-zone integration was carried out by using $7\times7\times1$ for the structural optimization, and $9\times9\times1$ for the total energy at Γ-centered grids. Spin-orbit coupling [55] and the vdW interactions were considered in all calculations, and the GGA+U method was used with the on-site repulsion parameter $U_{\text{eff}} = 4.00$ eV [34], where U is applied to the localized $3d$ orbitals of Mn. In order to better describe the topological properties, the Berry curvature and the anomalous Hall conductivity were estimated from a tight-binding Hamiltonian, constructed by the maximally localized Wannier functions using the WANNIER90 package [56,57].

III. STRUCTURAL STACKING AND STABILITY

Firstly, let us explore the stacking structures of different 2D material/MBT heterostructures. For the h-BN monolayer, as shown in Figs. 1(a)–1(c), three heterostructures of 2SL MBT and h-BN with different stacking can be designed. B_TN_H configuration means boron atoms are located at top sites above

TABLE I. Total magnetic moments M_{tot}, magnetic order, energy difference ΔE between FM and AFM/ferrimagnetic configurations, and Curie temperature T_C in 2SL MBT and various 2D vdW heterostructures.

Systems	M_{tot}/μ_B	Magnetic order	$\Delta E_{FM\text{-}AFM/FIM}$/meV	T_c/K
2SL MBT	0.0	AFM	1.6	
2SL MBT/h-BN (B_TN_H)	10.0	FM	−22.3	34
3SL MBT/h-BN (B_TN_H)	15.0	FM	−6.0	9
2SL MBT/h-BN (N_TB_H)	10.0	FM	−28.7	43
2SL MBT/h-BN (B_HN_H)	10.0	FM	−45.2	68
2SL MBT/MoS_2	10.0	FM	−15.1	23
2SL MBT/WSe_2	10.0	FM	−24.4	37
2SL MBT/α-In_2Se_3 (zincblende)	0.0	AFM	0.8	
2SL MBT/α-In_2Se_3 (wurtzite)	0.0	AFM	2.4	

Bi/Te columns and nitrogen atoms at hollow sites of 2SL MBT. Similarly N_TB_H means that nitrogen atoms are located at top sites above Bi/Te and boron atoms at hollow sites of MBT. And, in B_HN_H both boron and nitrogen atoms are located at hollows site of MBT. Our numerical calculations suggest that the B_TN_H is more stable since the total energy of B_TN_H is 15.0 and 27.7 meV/unit cell lower than B_HN_H and N_TB_H, respectively. In addition, we also constructed 2SL MBT/MoS_2, 2SL MBT/WSe_2 and 2SL MBT/α-In_2Se_3 and 3SL MBT/h-BN (B_TN_H) heterojunction models. For the different ferroelectric phases of (zincblende and wurtzite) α-In_2Se_3, two MBT/α-In_2Se_3 heterojunction models are displayed in Figs. 1(e) and 1(f). Experimentally MBT is easy to be oxidized and decompose in the air; thus, covering the MBT with the relatively stable 2D vdW material could significantly enhance the stability of MBT. Additionally, the interaction at the interface of the vdW heterojunction should retain the electronic structures and topological properties of MBT as we confirm in the following sections.

IV. MAGNETIC PROPERTIES

As found in previous studies, the relatively weak vdW interaction might also affect the interlayer magnetic coupling of heterostructures [11,26,58]. For example, a high-temperature ferromagnetic topological phase is generated in the Bi_2Se_3/EuS heterojunction due to the proximity effect [26]. In Table I, we first present the magnetic properties of 2SL MBT and confirm that the total energy of the antiferromagnetic order is 1.6 meV lower than ferromagnetic order, in agreement with previous study [33]. Except for the MBT/α-In_2Se_3 heterojunctions, our results demonstrate that interlayer ferromagnetic coupling takes place in the MBT/h-BN, MBT/MoS_2, and MBT/WSe_2 systems. And, the ferromagnetic coupling of MBT/h-BN (B_HN_H) is stronger, because the layer spacing between upper and lower MBT is smaller than that of B_TN_H and N_TB_H, by 0.08 and 0.04 Å, respectively. Meanwhile, all of the ferromagnetic phases host a magnetic moment about 5 μ_B/Mn atom, consistent with previous report as well [33]. On the other hand, the energies of antiferromagnetic states are about 0.8 meV, 2.4 meV less than the ferromagnetic states for the systems of α-In_2Se_3/MBT, whether zincblende or wurtzite phase. Especially for the MBT/h-BN (B_HN_H) heterojunction, the total energy of the ferromagnetic state is 45.2 meV lower than the antiferromagnetic state, corresponding to an estimated Curie temperature of about 68 K. For the MBT/MoS_2, MBT/WSe_2 systems, interlayer ferromagnetic coupling should also be achievable. In addition, we calculated the magnetic ground state of the MBT/h-BN heterojunctions by including the spin-orbit coupling, and found the out-of-plane magnetic structures are preferred over in-plane state by lowering energy about 0.42, 0.10, and 0.19 meV, respectively. Moreover, our calculations have approved that the interlayer ferromagnetic coupling is still preferred in the 3SL MBT/h-BN (B_TN_H) heterojunction system, where the energy of the ferromagnetic state is 6 meV lower than that of the ferrimagnetic (FIM) state. These results show that the coverage of 2D materials can help induce the occurrence of ferromagnetic phase transition. Therefore, such MBT/h-BN heterostructures have the potential to become candidate systems for high-temperature QAHE.

Next, we analyze the magnetic mechanisms of different 2D material/MBT heterostructures. Recently, some general rules have been proposed to study the interlayer magnetic coupling of vdW materials [58–60], especially for the MBT-family heterostructures. Li *et al.* attributed the interlayer ferromagnetic coupling to long-range superexchange interaction mediated by the *p* orbitals of nonmagnetic atoms across the vdW gap, like Te and Bi atoms in MBT [58]. In order to realize the interlayer ferromagnetic coupling, two prerequisites are indispensable in MBT-family materials. One is that the interlayer AFM coupling should be reduced while competing with FM couplings in the MBT-family materials. The other is related to the different 3*d* electrons occupations in the two different SLs of MBT. As shown in Fig. 2, the differential charge density of 2SL MBT and its heterostructures has been calculated according to the following formula [61]:

$$\Delta\rho = \rho(\text{total}) - \rho(\text{covering 2D materials}) - \rho(\text{upper MBT}) - \rho(\text{lower MBT}).$$

For the 2SL MBT system with the space symmetry, the charge accumulation or depletion in the upper SL and lower SL MBT are the same, as shown in Figs. 2(a) and 2(i). However, once covered by 2D materials, additional and different charge transfer between the upper and the lower SL MBT

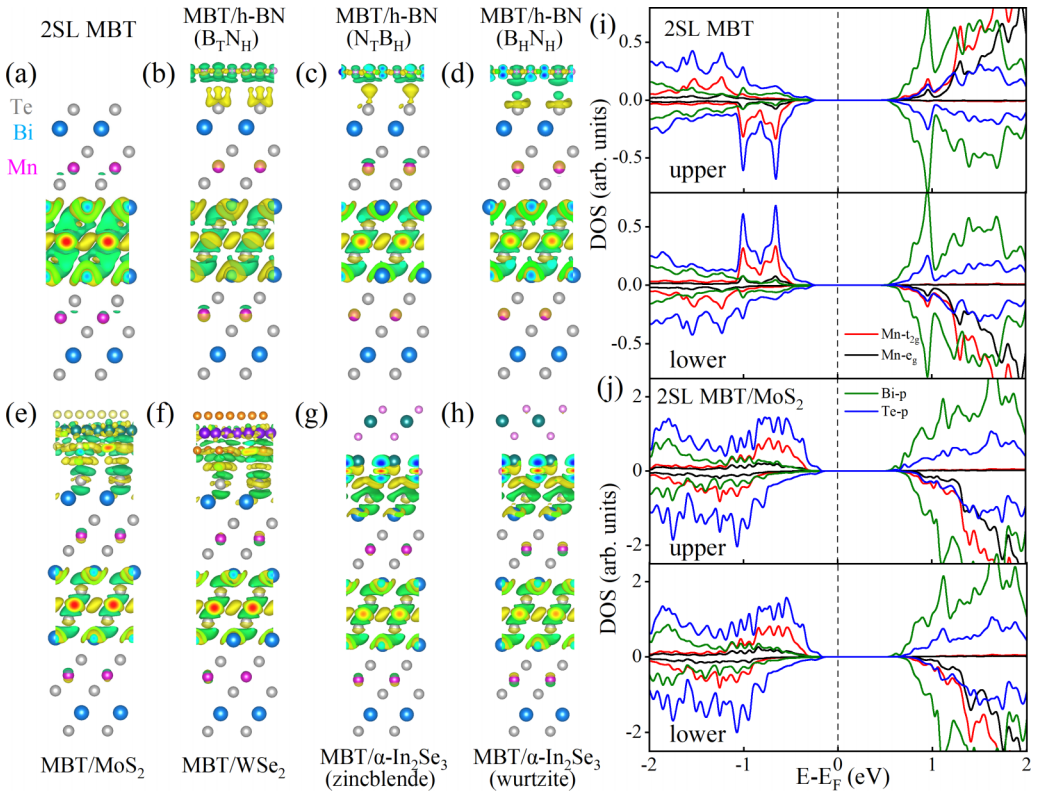

FIG. 2. Differential charge density in (a) 2SL MBT; and vdW heterostructures with top layer of (b) h-BN (B_TN_H), (c) h-BN (N_TB_H), (d) h-BN (B_HN_H), (e) MoS_2, (f) WSe_2, (g) α-In_2Se_3 (zincblende), and (h) α-In_2Se_3 (wurtzite). The yellow and green isosurfaces correspond to the accumulation and consumption of charge, respectively. Local density of states of (i) pristine 2SL MBT and (j) MBT/MoS_2. Te-*p*, Bi-*p*, and Mn-*d* orbitals (t_{2g} and e_g) in each SL of MBT are displayed.

happens in the MBT/2D heterojunction systems. In particular, we find that the cover layers have obviously weakened the interlayer AFM coupling between the upper and lower SL MBT. Especially for the MBT/h-BN, MBT/MoS_2, and MBT/WSe_2 systems, the charge changes of Mn atoms in the upper SL MBT are different from those in the lower SL MBT. These unequal charge changes of the Mn atoms in two different SL MBT could cause a new hopping channel between the upper and lower layers of Mn atoms in MBT/2D heterojunction, which is beneficial to the interlayer FM coupling with the weakened interlayer AFM coupling. Figure 2(j) shows the orbital resolved local density state of the MBT/MoS_2. It can be seen that the reduction of the *d*-orbital occupied state of the upper Mn atom leads to the formation of new hopping of t_{2g} and e_g, which is prone to induce ferromagnetic coupling [60,61]. The result presents inequivalent magnetic changes of the upper and lower layers of Mn atoms, indicating that the interlayer magnetic coupling is type I-II with preference to ferromagnetic coupling [58,59]. It is notable that the superexchange interaction [62,63] takes place in our systems, rather than the double-exchange interaction [64–66]. But, for the MBT/α-In_2Se_3 heterojunction, from Figs. 2(g) and 2(h), charge changes of Mn atoms in the upper SL MBT are nearly the same as those in the lower SL MBT. Hence, interlayer AFM coupling is still preferred although the interlayer AFM coupling has been weakened in the MBT/α-In_2Se_3 heterojunction.

V. BAND STRUCTURES AND QAHE

Figure 3 presents the band structures along high-symmetry lines for the investigated systems including 2SL MBT, 2SL MBT/h-BN in three different stacking ways, 2SL MBT/MoS_2, and 2SL MBT/WSe_2. One can see that all heterostructures have energy gap opening with different quantitative values at the Γ point. The energy gap of 2SL MBT/h-BN reaches 68 meV, which is only slightly smaller than the pristine 2SL MBT. In comparison, the energy gaps of other 2SL MBT heterojunctions are also smaller, but they all possess interlayer ferromagnetic coupling. Nevertheless, the energy gaps of these heterostructures are substantially larger than many typical systems that are possible to realize the high-temperature QAHE. Interestingly, 3SL MBT/h-BN (B_TN_H) heterojunction system also has a large nontrivial energy gap of 75 meV, as shown in Fig. 4(c).

Finally, we pay attention to the topology properties of these heterojunctions. We have verified that MBT/h-BN (B_TN_H) heterostructure has a nontrivial topological characteristic by calculating the Chern number, obtained from integration of the Berry curvature for the occupied valence bands [67]. Figures 4(a) and 4(c) display Berry curvature distribution along high-symmetry lines for 2SL and 3SL MBT/h-BN (B_TN_H) heterostructures, with large positive peaks near the Γ point and vanishing in other *k* space, respectively. Correspondingly, the total integration or the Hall conductance with the Fermi level lying inside the band gap must be nonzero. The

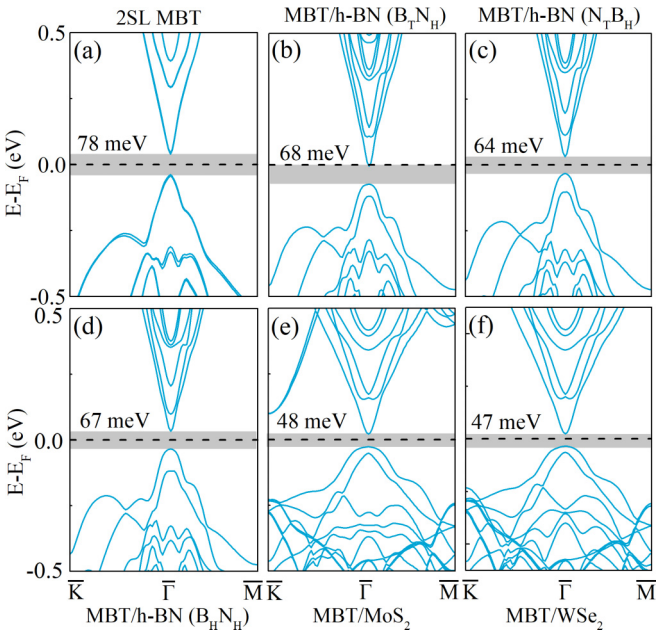

FIG. 3. Band structures of 2SL MBT and ferromagnetic heterostructures. (a) 2SL MBT, (b) 2SL MBT/h-BN (B_TN_H), (c) 2SL MBT/h-BN (N_TB_H), (d) 2SL MBT/h-BN (B_HN_H), (e) 2SL MBT/MoS_2, and (f) 2SL MBT/WSe_2. The dashed line denotes the Fermi level.

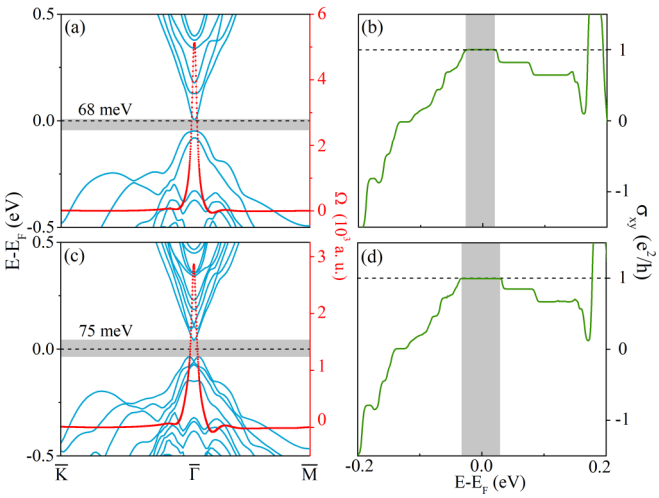

FIG. 4. Band structures along high-symmetry lines near the Γ point. The corresponding Berry curvatures are indicated in (a); Hall conductivity as a function of energy is in (b) for 2SL MBT/h-BN (B_TN_H) heterostructure; (c), (d) are for the 3SL MBT/h-BN (B_TN_H) heterostructure.

Hall conductance σ_{xy} results as a function of energy are shown in Figs. 4(b) and 4(d). The beautiful plateau $\sigma_{xy} = +e^2/h$ in the energy interval near the Fermi level corresponds to the Chern number of $C = 1$. These results thus confirm that the 2SL or 3SL MBT/h-BN (B_TN_H) heterostructure can achieve QAHE, and its observation temperature could be estimated to reach up to 34 K based on the previous calculation [68]. All these prove that the coverage of top 2D materials not only induces the occurrence of ferromagnetic phase transition, but also effectively protects the easily oxidized MBT. The important consequence is that we may have a large nontrivial energy gap to achieve high-temperature QAHE.

VI. SUMMARY

Based on first-principles calculations, we find that covering 2D systems such as h-BN, MoS_2, and WSe_2, onto MBT topological insulator cannot only protect it from degradation by the external environment, but also form intrinsically ferromagnetic vdW heterostructures to realize the high-temperature QAHE. Our results have shown that (1) interlayer ferromagnetic transition happens when a monolayer covers 2SL MBT with interlayer antiferromagnetic coupling; (2) band structures for both 2SL and 3SL MBT/h-BN heterostructures exhibit topologically nontrivial energy gaps around 64–75 meV, which host QAHE with a Chern number of $C = 1$; and (3) in particular, the excellent chemical stability of h-BN helps protect MBT in the air and maintain its outstanding electronic structure. Therefore, we expect covering 2D vdW materials onto MBT systems should be a very appropriate and straightforward approach for realizing high-temperature QAHE.

ACKNOWLEDGMENTS

This work was supported by the National Natural Science Foundation of China (Grants No. 51861145315, No. 11974098, No. 11974327, No. 11929401, and No. 12074241), the Independent Research and Development Project of State Key Laboratory of Advanced Special Steel, Shanghai Key Laboratory of Advanced Ferrometallurgy, Shanghai University (Grant No. SKLASS 2020-Z07), the Science and Technology Commission of Shanghai Municipality (Grants No. 19DZ2270200, No. 19010500500, and No. 20501130600), the Natural Science Foundation of Hebei Province (Grant No. A2019205037), and High Performance Computing Center, Shanghai University.

[1] F. D. M. Haldane, Phys. Rev. Lett. **61**, 2015 (1988).
[2] K. He, Y. Wang, and Q.-K. Xue, Natl. Sci. Rev. **1**, 38 (2014).
[3] C.-X. Liu, S.-C. Zhang, and X.-L. Qi, Annu. Rev. Condens. Matter Phys. **7**, 301 (2016).
[4] K. He, Y. Wang, and Q.-K. Xue, Annu. Rev. Condens. Matter Phys. **9**, 329 (2018).
[5] L. Bellaiche, W. Ren, and S. Singh, Phys. Rev. B **88**, 161102(R) (2013).
[6] Y. Ren, Z. Qiao, and Q. Niu, Rep. Prog. Phys. **79**, 066501 (2016).
[7] S.-C. Wu, G. Shan, and B. Yan, Phys. Rev. Lett. **113**, 256401 (2014).

[8] R. Yu, W. Zhang, H.-J. Zhang, S.-C. Zhang, X. Dai, and Z. Fang, Science **329**, 61 (2010).

[9] M. Mogi, R. Yoshimi, A. Tsukazaki, K. Yasuda, Y. Kozuka, K. Takahashi, M. Kawasaki, and Y. Tokura, Appl. Phys. Lett. **107**, 182401 (2015).

[10] H. Jiang, Z. Qiao, H. Liu, and Q. Niu, Phys. Rev. B **85**, 045445 (2012).

[11] Z. Qiao, W. Ren, H. Chen, L. Bellaiche, Z. Zhang, A. H. MacDonald, and Q. Niu, Phys. Rev. Lett. **112**, 116404 (2014).

[12] M. Onoda and N. Nagaosa, Phys. Rev. Lett. **90**, 206601 (2003).

[13] Z. Qiao, S. A. Yang, W. Feng, W.-K. Tse, J. Ding, Y. Yao, J. Wang, and Q. Niu, Phys. Rev. B **82**, 161414(R) (2010).

[14] S. Qi, R. Gao, M. Chang, Y. Han, and Z. Qiao, Phys. Rev. B **101**, 014423 (2020).

[15] S. Qi, R. Gao, M. Chang, T. Hou, Y. Han, and Z. Qiao, Phys. Rev. B **102**, 085419 (2020).

[16] K. F. Garrity and D. Vanderbilt, Phys. Rev. Lett. **110**, 116802 (2013).

[17] J.-Y. You, C. Chen, Z. Zhang, X.-L. Sheng, S. A. Yang, and G. Su, Phys. Rev. B **100**, 064408 (2019).

[18] C. Fang, M. J. Gilbert, and B. A. Bernevig, Phys. Rev. Lett. **112**, 046801 (2014).

[19] S. Qi, Z. Qiao, X. Deng, E. D. Cubuk, H. Chen, W. Zhu, E. Kaxiras, S. B. Zhang, X. Xu, and Z. Zhang, Phys. Rev. Lett. **117**, 056804 (2016).

[20] P. Haazen, J.-B. Laloë, T. Nummy, H. Swagten, P. Jarillo-Herrero, D. Heiman, and J. Moodera, Appl. Phys. Lett. **100**, 082404 (2012).

[21] Y. S. Hor, P. Roushan, H. Beidenkopf, J. Seo, D. Qu, J. G. Checkelsky, L. A. Wray, D. Hsieh, Y. Xia, S.-Y. Xu, D. Qian, M. Z. Hasan, N. P. Ong, A. Yazdani, and R. J. Cava, Phys. Rev. B **81**, 195203 (2010).

[22] C.-Z. Chang, J. Zhang, X. Feng, J. Shen, Z. Zhang, M. Guo, K. Li, Y. Ou, P. Wei, L.-L. Wang, Z. Ji, Y. Feng, S. Ji, X. Chen, J. Jia, X. Dai, Z. Fang, S.-C. Zhang, K. He, Y. Wang, L. Liu, X. Ma, and Q.-K. Xue, Science **340**, 167 (2013).

[23] Y. Ou, C. Liu, G. Jiang, Y. Feng, D. Zhao, W. Wu, X. X. Wang, W. Li, C. Song, L. L. Wang, W. Wang, W. Wu, and Y. Wang, Adv. Mater. **30**, 1703062 (2018).

[24] K. He and Q.-K. Xue, Natl. Sci. Rev. **6**, 202 (2019).

[25] X.-L. Qi, T. L. Hughes, and S.-C. Zhang, Phys. Rev. B **78**, 195424 (2008).

[26] F. Katmis, V. Lauter, F. S. Nogueira, B. A. Assaf, M. E. Jamer, P. Wei, B. Satpati, J. W. Freeland, I. Eremin, D. Heiman, P. Jarillo-Herrero, and J. S. Moodera, Nature (London) **533**, 513 (2016).

[27] M. M. Otrokov, T. V. Menshchikova, M. G. Vergniory, I. P. Rusinov, A. Y. Vyazovskaya, Y. M. Koroteev, G. Bihlmayer, A. Ernst, P. M. Echenique, A. Arnau, and E. V. Chulkov, 2D Mater. **4**, 025082 (2017).

[28] Y. Hou, J. Kim, and R. Wu, Sci. Adv. **5**, eaaw1874 (2019).

[29] C. Tang, C.-Z. Chang, G. Zhao, Y. Liu, Z. Jiang, C.-X. Liu, M. R. McCartney, D. J. Smith, T. Chen, J. S. Moodera, and J. Shi, Sci. Adv. **3**, 700307 (2017).

[30] C. Lee, F. Katmis, P. Jarillo-Herrero, J. S. Moodera, and N. Q. Gedik, Nat. Commun. **7**, 12014 (2016).

[31] L. Alegria, H. Ji, N. Yao, J. Clarke, R. J. Cava, and J. R. Petta, Appl. Phys. Lett. **105**, 053512 (2014).

[32] Z. Jiang, C.-Z. Chang, C. Tang, P. Wei, J. S. Moodera, and J. Shi, Nano Lett. **15**, 5835 (2015).

[33] J. Li, Y. Li, S. Du, Z. Wang, B.-L. Gu, S.-C. Zhang, K. He, W. Duan, and Y. Xu, Sci. Adv. **5**, eaaw5685 (2019).

[34] Y. Gong, J. Guo, J. Li, K. Zhu, M. Liao, X. Liu, Q. Zhang, L. Gu, L. Tang, X. Feng, D. Zhang, W. Li, C. Song, L. Wang, P. Yu, X. Chen, Y. Wang, H. Yao, W. Duan, Y. Xu, S.-C. Zhang, X. Ma, Q.-K. Xue, and K. He, Chin. Phys. Lett. **36**, 076801 (2019).

[35] H. Fu, C.-X. Liu, and B. Yan, Sci. Adv. **6**, eaaz0948 (2020).

[36] C. X. Trang, Q. Li, Y. Yin, J. Hwang, G. Akhgar, I. D. Bernardo, A. Grubišić-Čabo, A. Tadich, M. S. Fuhrer, S. Mo, N. Medhekar, and M. T. Edmonds, ACS Nano **15**, 13444 (2021).

[37] H. Sun, B. Xia, Z. Chen, Y. Zhang, P. Liu, Q. Yao, H. Tang, Y. Zhao, H. Xu, and Q. Liu, Phys. Rev. Lett. **123**, 096401 (2019).

[38] Y. Deng, Y. Yu, M. Z. Shi, Z. Guo, Z. Xu, J. Wang, X. H. Chen, and Y. Zhang, Science **367**, 895 (2020).

[39] Y. Yuan, X. Wang, H. Li, J. Li, Y. Ji, Z. Hao, Y. Wu, K. He, Y. Wang, Y. Xu, W. Duan, W. Li, and Q.-K. Xue, Nano Lett. **20**, 3271 (2020).

[40] A. Zeugner, F. Nietschke, A. U. Wolter, S. Gaß, R. C. Vidal, T. R. Peixoto, D. Pohl, C. Damm, A. Lubk, R. Hentrich, S. K. Moser, C. Fornari, C. H. Min, S. Schatz, K. Kißner, M. Ünzelmann, M. Kaiser, F. Scaravaggi, B. Rellinghaus, K. Nielsch, C. Hess, B. Büchner, F. Reinert, H. Bentmann, O. Oeckler, T. Doert, M. Ruck, and A. Isaeva, Chem. Mater. **31**, 2795 (2019).

[41] F. Hou, Q. Yao, C.-S. Zhou, X.-M. Ma, M. Han, Y.-J. Hao, X. Wu, Y. Zhang, H. Sun, C. Liu, Y. Zhao, Q. Liu, and J. Lin, ACS Nano **14**, 11262 (2020).

[42] X. Ling, W. Fang, Y.-H. Lee, P. T. Araujo, X. Zhang, J. F. Rodriguez-Nieva, Y. Lin, J. Zhang, J. Kong, and M. S. Dresselhaus, Nano Lett. **14**, 3033 (2014).

[43] M. Morscher, M. Corso, T. Greber, and J. Osterwalder, Surf. Sci. **600**, 3280 (2006).

[44] K. M. McCreary, A. T. Hanbicki, J. T. Robinson, E. Cobas, J. C. Culbertson, A. L. Friedman, G. G. Jernigan, and B. T. Jonker, Adv. Funct. Mater. **24**, 6449 (2014).

[45] Y. You, X.-X. Zhang, T. C. Berkelbach, M. S. Hybertsen, D. R. Reichman, and T. F. Heinz, Nat. Phys. **11**, 477 (2015).

[46] N. Gillgren, D. Wickramaratne, Y. Shi, T. Espiritu, J. Yang, J. Hu, J. Wei, X. Liu, Z. Mao, and K. Watanabe, 2D Mater. **2**, 011001 (2014).

[47] T. Hu and J. Hong, ACS Appl. Mater. Interf. **7**, 23489 (2015).

[48] G. Kresse and J. Furthmüller, Phys. Rev. B **54**, 11169 (1996).

[49] P. E. Blöchl, Phys. Rev. B **50**, 17953 (1994).

[50] J. P. Perdew, J. A. Chevary, S. H. Vosko, K. A. Jackson, M. R. Pederson, D. J. Singh, and C. Fiolhais, Phys. Rev. B **46**, 6671 (1992).

[51] B. Li, D. Pajerowski, S. Riberolles, L. Ke, J. Yan, and R. McQueeney, arXiv:2007.08468.

[52] B. Lian, Z. Liu, Y. Zhang, and J. Wang, Phys. Rev. Lett. **124**, 126402 (2020).

[53] C. Xiao, J. Tang, P. Zhao, Q. Tong, and W. Yao, Phys. Rev. B **102**, 125409 (2020).

[54] D. Zhang, M. Shi, T. Zhu, D. Xing, H. Zhang, and J. Wang, Phys. Rev. Lett. **122**, 206401 (2019).

[55] S. Steiner, S. Khmelevskyi, M. Marsmann, and G. Kresse, Phys. Rev. B **93**, 224425 (2016).

[56] A. A. Mostofi, J. R. Yates, Y.-S. Lee, I. Souza, D. Vanderbilt, and N. Marzari, Comput. Phys. Commun. **178**, 685 (2008).

[57] M. L. Sancho, J. L. Sancho, J. L. Sancho, and J. Rubio, J. Phys. F: Met. Phys. **15**, 851 (1985).

[58] Z. Li, J. Li, K. He, X. Wan, W. Duan, and Y. Xu, Phys. Rev. B **102**, 081107(R) (2020).
[59] J. Xiao and B. Yan, 2D Mater. **7**, 045010 (2020).
[60] W. Zhu, C. Song, L. Liao, Z. Zhou, H. Bai, Y. Zhou, and F. Pan, Phys. Rev. B **102**, 085111 (2020).
[61] Y. Han, S. Sun, S. Qi, X. Xu, and Z. Qiao, Phys. Rev. B **103**, 245403 (2021).
[62] M. Gilleo, Phys. Rev. **109**, 777 (1958).
[63] J. Yamashita and J. Kondo, Phys. Rev. **109**, 730 (1958).
[64] P. W. Anderson and H. Hasegawa, Phys. Rev. **100**, 675 (1955).
[65] P.-G. De Gennes, Phys. Rev. **118**, 141 (1960).
[66] C. Wang, X. Zhou, Y. Pan, J. Qiao, X. Kong, C.-C. Kaun, and W. Ji, Phys. Rev. B **97**, 245409 (2018).
[67] Y. Yao, L. Kleinman, A. H. MacDonald, J. Sinova, T. Jungwirth, D.-S. Wang, E. Wang, and Q. Niu, Phys. Rev. Lett. **92**, 037204 (2004).
[68] M. M. Otrokov, I. P. Rusinov, M. Blanco-Rey, M. Hoffmann, A. Y. Vyazovskaya, S. V. Eremeev, A. Ernst, P. M. Echenique, A. Arnau, and E. V. Chulkov, Phys. Rev. Lett. **122**, 107202 (2019).